Relation between PEEK Semicrystalline Morphology and Its Subglass Relaxations and Glass Transition

Alain Jonas*,† and Roger Legras

Laboratoire de Physico-Chimie et Physique des Matériaux and Laboratoire de Physique et de Chimie des Hauts Polymères, Université Catholique de Louvain, Place Croix du Sud 1, B-1348 Louvain-la-Neuve, Belgium

Received April 29, 1992; Revised Manuscript Received October 5, 1992

ABSTRACT: The PEEK glass transition (α-relaxation) is studied as a function of polymer semicrystalline morphology, characterized by small-angle X-ray scattering. An inverse relationship is observed between glass transition temperature and amorphous interlayer thickness. This is interpreted in terms of configurational entropy differences in the amorphous regions of semicrystalline samples, as compared to a bulk amorphous sample. The existence of so-called rigid amorphous fractions is shown to result partly from these entropy differences. The PEEK subglass transitions have also been studied. The highly-localized wagging of the polar bridges corresponding to the γ-relaxation is insensitive to ageing history and details of the semicrystalline morphology. The combination of the γ-wagging with phenyl flips results in the appearance of the β-relaxation. The energy barriers controlling the onset of β-motions are intermolecular in nature. Thus, perturbations of the environment of the relaxing moiety (water content, ageing history, details of the semicrystalline morphology) affect the β-relaxation.

1. Introduction

Poly(oxy-1,4-phenyleneoxy-1,4-phenylenecarbonyl-1,4-phenylene) (PEEK) is a semicrystalline polymer having outstanding mechanical and thermal properties, along with a high solvent resistance. In view of the technological importance of this polymer, numerous research papers on PEEK have been published in the past 10 years, most of them focusing on engineering properties and crystallization kinetics. Some details on PEEK can be found in a recent review.[1]

PEEK presents interesting features, which render it particularly well suited to progress into the general understanding of semicrystalline polymer morphology. Its fully para-aromatic chain structure is straightforward, with no pendant group nor phenyl ortho or meta substitution. It can be easily crystallized, and the polymer degradation during processing can be controlled.[2] The available range of crystallinity spans from 0 to ~40 vol %, while quoted lamellar thicknesses are between 2 and 6 nm.[3-6] Thus, a wide range of crystallinities and morphologies can be accessed. However, the semicrystalline architecture of PEEK is still relatively poorly known. Important topics like the probable existence of a crystalline/amorphous interphase have not yet been much explored for this polymer.

The existence of an interfacial layer connecting crystallites to the liquid-like amorphous phase in semicrystalline polymers has been predicted or observed by various authors. Numerical computations on lattice models,[7-10] initially performed to contribute to the much debated issue of adjacent reentry and tight folding,[11] have shown that the crystal order needs some distance to be fully dissipated in the amorphous region, this distance being dependent on the chain bending energy and the crystalline chain tilt angle relative to the lamellar surface. Quantitative experimental determinations of the relative amounts of crystalline, liquid-like, and interfacial transition regions were performed for PE by Strobl and Hagedorn[12] using Raman specroscopy. This technique was later used by Mandelkern et al.,[13,14] together with a determination of the crystalline lamellar thickness (l_c) by analysis of the Raman longitudinal acoustical mode, to measure interfacial and liquid-like region thicknesses in melt-crystallized PE. Values around 1.5–2.5 nm were obtained. Evidence for an interfacial region was also gained from small-angle X-ray and neutron scattering experiments performed on blends of compatible polymers, from which only one can be crystallized.[15-17] The resulting estimations for the thickness of the interfacial region of poly(ethylene oxide) and poly(vinylidene fluoride) were respectively 1.5 and 2.5 nm.

However, the bulk of experimental results supporting the interphase existence comes from techniques probing motions inside the amorphous regions. Conformational differences inside the liquid-like phase and the interphase give rise to different relaxation times. Solid-state NMR,[18] dynamic mechanical spectroscopy, and dielectric spectroscopy[19-21] were widely used in this respect, due to their relative widespread availability. However, most of the published works do not characterize the polymer morphology further than specifying a degree of crystallinity, a rather crude description of microstructure. Creep experiments and ageing studies[22] also support the three-region[23] picture of semicrystalline polymers.

The present paper is devoted to the description of the PEEK subglass relaxations and glass transition as a function of its semicrystalline morphology. There are two aims to this study: first, to further our understanding of PEEK relaxations, and second, to contribute to forge a better picture of the semicrystalline morphology of this polymer. Techniques used are dielectric spectroscopy (DS) for the study of the PEEK subglass relaxations as a function of temperature and frequency and dynamic mechanical spectroscopy (DMA) and differential scanning calorimetry (DSC) for the characterization of the polymer glass transition. The PEEK morphology has been investigated by small-angle X-ray scattering (SAXS).

There have been only a few studies devoted to the subglass relaxations of PEEK, none of them being concerned about PEEK morphology. Sasuga and Hagiwara[24] investigated the influence of electron beam irradiation on the PEEK dynamic mechanical properties. They analyzed the β (first subglass[25]) mechanical relaxation in terms of two overlapping processes (~230 and ~190 K, 1 Hz); a

† Research Assistant of the Belgian National Fund for Scientific Research.

0024-9297/93/2226-0813$04.00/0

Table I
Nomenclature, Processing Conditions, Volume Degree of Crystallinity, and Characterization Techniques Used for Each Sample of This Study

sample name	processing thermal history	vol crystallinity (ϕ)	characterization techniques
Q	quenched from 673 K in water	0.02	DSC, DMA, DS
G/423	sample Q + 30-min annealing at 423 K, then quenched	0.08	DSC, DMA
G/453	sample Q + 30-min annealing at 453 K, then quenched	0.22	DSC, DMA, SAXS, DS
G/493	sample Q + 30-min annealing at 493 K, then quenched	0.26	DSC, DMA, SAXS
G/533	sample Q + 30-min annealing at 533 K, then quenched	0.26	DSC, DMA, SAXS
G/573	sample Q + 30-min annealing at 573 K, then quenched	0.28	DSC, DMA, SAXS
M/293	fast cooling from 673 K to room temperature	0.10	DS
M/393	fast cooling from 673 to 393 K, where the sample is held 10 min, then quenched	0.25	DSC, DMA, SAXS
M/423	fast cooling from 673 to 423 K, where the sample is held 30 min, then quenched	0.26	DSC, DMA, SAXS
M/453	fast cooling from 673 to 453 K, where the sample is held 30 min, then quenched	0.27	DSC, DMA, SAXS
M/573	fast cooling from 673 to 573 K, where the sample is held 15 min, then quenched	0.29[a]	DSC, DMA, SAXS, DS
M/SC	slow cooling from 673 K to room temperature (heating power of the press turned off)	0.40[b]	DSC, DMA, SAXS

[a] A value previously reported in the literature[37] was in error. [b] This value is overestimated due to neglect of the variation of the crystal density with crystallization temperature.

third process appears at the lower temperature side of this broad loss peak in specimens containing water traces (β_w, ~170 K, 1 Hz). The existence of a fourth process at still lower temperatures has been detected by Ahlborn[26] (γ, ~118 K, 7 Hz). The molecular motions from which these relaxations originate are still largely unknown. The PEEK glass transition has been studied by DSC[27] and by DS.[28] Variations in the location and broadness of the glass transition were observed with changes in the PEEK degree of crystallinity.

Since the bulk crystallization of PEEK has been found to be similar in many respects to that of poly(ethylene terephthalate) (PET),[3] it is logical to infer that the influence crystallites exert on the amorphous regions must bear also some similarity for both polymers. The PET glass transition (and the α_a-relaxation associated with the same segmental motions) has been well characterized;[29-32] the relaxation process first shifts toward higher temperatures as crystallinity increases, and then a reversal of the trend is observed for higher crystallinities. This behavior was tentatively interpreted[31,32] as due to changes in the amorphous layer thickness between lamellae. However, no independent measurement of this thickness was performed. Simultaneously, the broadness of the relaxation in the frequency domain increases strongly, while its asymmetry decreases, presumably reflecting the restriction of segmental motions due to the crystallization. No such significant changes in the shape of the sub-T_g process were observed; this is in agreement with the general belief that the molecular motions giving rise to this process are in localized nature. However, the temperature location of this process has been described by Illers and Breuer[31] as morphology-sensitive, while others[29,30,32] claimed that the morphology has no or very little influence on this location.

Finally, this study being devoted to the amorphous phase, it has to take into account the nonequilibrium character of this phase, which is reflected by the ageing phenomenon. A few works have been reported on PEEK physical ageing,[33-35] but the range of temperature scanned is limited to ~30 K below T_g. Fortunately, impresssive amounts of data on polymer ageing have been published by Struik.[22] It has been shown that ageing occurs in a large temperature range from roughly the β-relaxation temperature (T_β) up to the glass transition temperature (T_g). Since T_β is located below room temperature for most polymers (and also for PEEK), the material must be suspected of evolution even during storage at room temperature. The thermal history of the semicrystalline sample below its T_g affects the measured glass transition. However, the location of subglass relaxations has been claimed[36] to be hardly influenced by changes in sample thermal history.

After the Experimental Section, results related to the SAXS determination of PEEK morphology, to its glass transition, and to its subglass relaxations will be given. In the final section, the information provided by the different techniques will be gathered and discussed.

2. Experimental Section

Sample Preparation. PEEK sheets (~200 μm thick) were prepared from dry commercial powder (I.C.I. grade 150P, measured[2] M_n = 10 300, M_w = 26 800) as described elsewhere.[37] Basically, two series of samples were prepared, either by annealing at T_c (above T_g) quenched amorphous plates (samples isothermally crystallized from the glass (G)) or by transferring the molten polymer to a press held at T_c (samples crystallized from the melt (M)). Most of the samples were kept at T_c during a time long enough to ensure complete primary crystallization (spherulite impingement), as judged from prior DSC crystallization kinetics measurements. However, sample W was not crystallized, and sperulites did not impinge in samples G/423 and M/293 due to the low crystallization temperature or fast cooling rate, respectively. After crystallization, the samples were directly quenched in water to ensure the same thermal history in the T_g range. An exception to this rule is sample M/SC, which was obtained by slow cooling from the molten state to room temperature. Table I gives the nomenclature and processing conditions of the samples investigated.

Crystallinity Determination. Specific weights (ρ) were determined by weighing the samples in air and in water. Volume crystallinity, ϕ, was computed from the specific weight of the pure amorphous phase (ρ_a = 1.263 g cm^{-3}) and of the crystal phase (ρ_c = 1.4 cm^{-3}). Some variation of ρ_c with crystallization temperature has been reported in the literature. A brief discussion of this phenomenon, and evidence to use 1.4 cm^{-3} as the mean value for ρ_c can be found elsewhere.[38] The sample degree of crystallinity is reported in Table I.

Small-Angle X-ray Scattering. SAXS patterns were recorded in an evacuated Kratky camera (slit collimation) with a Braun position-sensitive proportional counter, using Cu Kα radiation. After background subtraction, the recorded curves were smoothed using a second-derivative-based moving-average smoothing procedure[39] and desmeared by simple resolution of the triangular system resulting from the discretization of the

convolution equation, assuming infinite slit length. The curves were finally Lorentz corrected. One-dimensional correlation functions were directly computed from the smeared intensities; this required extrapolation of the intensity to zero angle. A simple linear extrapolation was used; the roughness of this approximation does not allow one to consider correlation functions as significant for distances greater than 15–20 nm.

Differential Scanning Calorimetry. Specific heat (c_p) determination of the samples was performed between 323 and 573 K in a Perkin-Elmer DSC2 operated at 10 K min^{-1}. Temperature was calibrated with indium and tin, and the ordinate was calibrated with a sapphire standard. Due to the small film thickness, only ~15 mg of sample could be measured at a time (heat transfer problems prevent realization of thicker morphology-controlled films). To characterize the glass transition, the specific heats below (respectively above) the specific heat jump had to be extrapolated upward (respectively downward). Thus, the sample specific heat below T_g was fit to the "solid"[40] PEEK specific heat multiplied by an adjustable constant which takes into account some experimental errors (sample weight etc.) and the small difference between the crystalline and glassy polymer specific heats at these temperatures. The "solid" PEEK specific heat was computed following the addition scheme procedure described by Cheng et al.[41] In all cases, this fit was performed without problems, the adjustable constant being equal to 1 within less than 2%. The specific heat above the transition was fit to a linear combination between the computed "solid" PEEK specific heat and the experimental liquid specific heat reported by Cheng and Wunderlich.[42] Such a fit was found possible only in a limited temperature range above T_g. Positive or negative deviations from the expected relation occur above a given temperature T_R. These deviations result from changes of c_p due to related changes in the degree of crystallinity during the heating scan,[37] from exothermic or endothermic processes like crystallization of amorphous sheets or the low temperature melting endotherm observed in isothermally-crystallized PEEK,[37] or from changes in the so-called rigid amorphous fraction,[43] i.e., progressive unfreezing of constrained amorphous segments. In most cases, the extrapolation of the specific heat above the transition is not straightforward. Once the two "base lines" are drawn, they are used to compute $T_{g,DSC}$, the temperature corresponding to half the transition specific heat jump, and Δc_p, the transition specific heat jump extrapolated at $T_{g,DSC}$, in accordance with previous works.[43] The rigid amorphous fraction ($\phi_{r,am}$) is then computed,[43] using

$$\phi_{r,am} = 1 = \Delta c_p/\Delta c_{p,a} - \psi \quad (1)$$

with ψ the degree of crystallinity by weight and $\Delta c_{p,a}$ the specific heat jump of a pure amorphous sample at $T_{g,DSC}$, calculated from the computed "solid" PEEK specific heat and the experimental liquid specific heat reported by Cheng and Wunderlich.[42] The precision on $\phi_{r,am}$ is small, due to the aforementioned difficulty in evaluating Δc_p with precision, to be the low amounts of sample scanned, and to amplification of relative errors when computing differences.

Dynamic Mechanical Analysis. Dynamic mechanical analysis was performed in the tension mode with a Rheometrics RSA II. A 1-Hz dynamic deformation varying between 0.02 and 0.3% (following temperature and crystallinity) was superimposed on a static deformation equal to 1.5 times the amplitude of the dynamic deformation. In the glass transition region, the sample was heated by 1 K steps and allowed to equilibrate during 1 min before measuring the storage (E') and loss (E'') moduli. $T_{g,DMA}$ was defined as the temperature at which E'' reaches its maximum. The samples were measured within 1 month after their fabrication and were not dried before the experiments, in order to minimize ageing. The small amounts of absorbed water are no problem since T_g is high enough to allow water desorption during the scan from 323 K up to T_g.

Dielectric Spectroscopy. The measuring system is a homemade cryostatic device described elsewhere.[44] Available frequencies range from 200 Hz to 100 kHz, although inductive losses in the bridge decrease the precision of the measurement above 10 kHz. The system can be evacuated down to 3.5×10^{-3} Pa (2.5×10^{-5} Torr) at room temperature. Typical relative precisions are ~2% on tan δ and better than 0.01% on ϵ_r. However, absolute precisions are much lower for ϵ_r, due to uncertainties in the determination of geometric dimensions (~10%). The same holds for the imaginary part of the relative permittivity, ϵ_i. The relative precision of this parameter is the same as for tan δ.

(a) Sample Preparation. Thin gold electrodes are first sputtered on both sides of a sample plate. The sample is then cut in the form of a 3-cm-diameter disk; on one side, the deposited electrode is split into a guard ring and a guarded electrode of 2-cm diameter. The gap between the guarded electrode and the guard, measured with an optical microscope, is of the order of 50 μm.

(b) Water Uptake Studies and Samples Thermal History. Electrode-coated samples were immersed in boiling demineralized water. They were periodically removed from the water, gently swept, and weighed, and their dielectric permittivity was measured at room temperature. After water uptake saturation, the same samples were placed under vacuum at 373 K. They were again periodically weighed and their dielectric properties measured.

To observe the dielectric temperature behavior of water-saturated samples, samples were saturated by immersion in boiling water during 2 days, the samples were then placed into the cryostatic system, and the Dewar was filled with liquid nitrogen. Once the cryostat temperature had fallen below 250 K (30 min after placement of the sample inside the cell), pumping was started; this ensured minimal water desorption.

To observe the effects of drying on the dielectric temperature behavior of PEEK, samples in equilibrium with the laboratory atmosphere were placed into the cryostat; the cryostat was evacuated, and the system was cooled when the pressure had decreased below ~1×10^{-1} Pa. Dielectric properties were then measured from 77 K to room temperature, where the sample was left for a couple of days. During this time, pressure continually dropped due to progressive water desorption. The sample was cooled again, and dielectric properties were measured. The procedure was repeated several times until the pressure reached 3.5×10^{-3} Pa; this corresponds to the lower limit of pressure that can be obtained in our system, and no changes in the dielectric thermal behavior can be observed for longer pumping times at this pressure.

Finally, dielectric properties were measured on so-called "dry" samples. This refers to samples having been placed for at least 2 days at 373 K in the primary vacuum and then having been mounted in the cryostat and kept at room temperature in the cryostat until the pressure reached 3.5×10^{-3} Pa. The time required to attain this value varies, presumably depending on the time elapsed while mounting the sample in the cryostat. This time is always greater than 1 week.

3. Results

3.1. SAXS Morphological Characterization. The SAXS patterns of the samples have been analyzed by three different ways. First, the Bragg law was applied to the maximum value of the desmeared and Lorentz-corrected intensity, in order to obtain the long period L_{Bragg}. A recent theoretical analysis[45] has shown that such a Bragg analysis yields long periods up to 15% greater than the computed mean values, in accordance with the assumption[46] that this analysis gives the weight average of the long period. From the knowledge of the volume crystallinity of the samples, the crystalline core thickness, $l_{c,Bragg}$, and the amorphous layer thickness, $l_{a,Bragg}$, were computed. The results of this simple analysis are presented in Table II, columns II and III. Second, the one-dimensional correlation function was analyzed using the Strobl procedure.[47] The resulting long period, L_γ, and the crystalline core thickness, $l_{c,\gamma}$, are presented in Table II, columns IV and V. This analysis is thought to give number averages[46] for the thickness. Third, the Lorentz-corrected desmeared curves were fit to the general (one-dimensional) paracrystalline model using as thickness distributions for the crystalline cores and the amorphous layers two independent asymmetric Reinhold distributions.[48] This analysis is the most controversial, since there are no a priori reasons

Table II
Long Period (L) and Crystalline Core Thickness (l_c) of the PEEK Samples[a]

sample name	L_{Bragg} (nm)	$l_{c,Bragg}$ (nm)	L_γ (nm)	$l_{c,\gamma}$ (nm)	L_R (nm)	$l_{c,R}$ (nm)
G/453	10.09	2.25	9.93	2.38	12.63	2.66
G/493	11.06	2.84	10.78	2.52	12.93	2.87
G/533	12.28	3.17	11.39	2.80	14.10	3.21
G/573	14.60	4.03	14.01	3.34	16.13	4.12
M/393	12.73	3.13	11.70	3.07	14.29	3.45
M/423	12.74	3.29	11.62	3.00	14.10	3.51
M/453	12.65	3.47	11.65	3.09	13.82	3.52
M/573	15.70	4.57	14.43	3.79	16.63	4.71
M/SC	14.89	5.94	14.01	3.65	15.20	4.79

[a] Columns II and III refer to a simple Bragg analysis of the SAXS patterns, columns IV and V to a Strobl analysis of the correlation function γ, and columns VI and VII to a direct fit of the SAXS patterns with a one-dimensional general paracrystalline model.

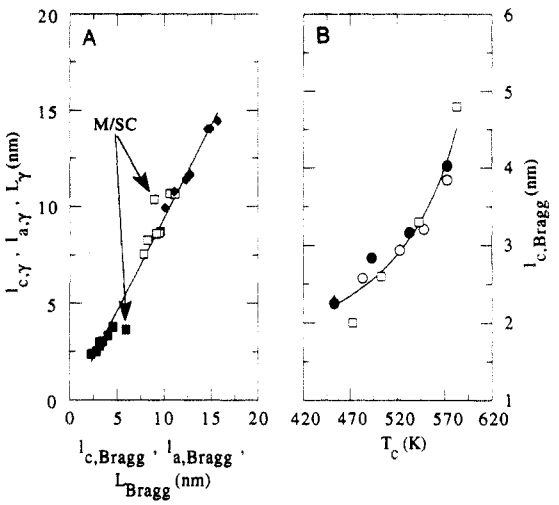

Figure 1. (A) Plot of the SAXS-determined thicknesses of the crystalline core (l_c, ■) and amorphous interlayer (l_a, □) and the long distance (L, ♦) using the Strobl analysis of the correlation function γ versus the same parameters obtained from a simple Bragg analysis. (B) Evolution of the PEEK crystalline core thickness ($l_{c,Bragg}$) with crystallization temperature T_c (crystallization time less than ~2 h). (●) Isothermally-crystallized samples of this study; literature data: (□) ref 3; (○) ref 4; (△) ref 5.

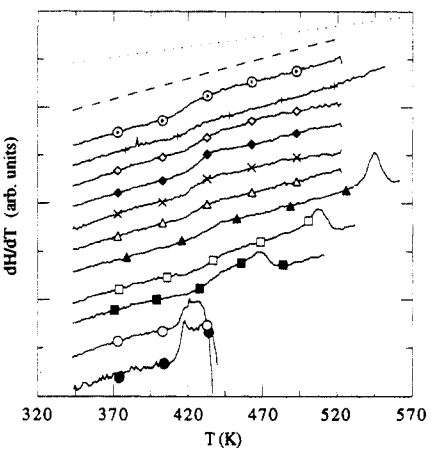

Figure 2. Evolution with temperature of the temperature derivative of the sample enthalpy (dH/dT). The curves have been displaced vertically for clarity. Dashed line, computed[41] solid PEEK specific heat; dotted line, liquid PEEK specific heat.[42] For the nomenclature of samples, refer to Table I. (●) Q; (○) G/423; (■) G/453; (□) G/493; (▲) G/533; (△) G/573; (×) M/393; (♦) M/423; (◇) M/453; (+) M/573; (⊙) M/SC. (All points are not plotted on the figure.)

to choose any type of distribution. It was decided to choose the Reinhold distribution only because its asymmetry allows one to avoid negative thickness problems, which generally arise when considering Gaussian distributions. The mean values computed from this model for the long period, L_R, and for the crystalline core thickness, $l_{c,R}$, are given in Table II, columns VI and VII.

Figure 1A displays l_c, l_a, and L, derived from the analysis of the correlation function, versus the same parameters extracted from the simple Bragg analysis. A good correlation between the results obtained by both types of analysis is obtained, except for the sample crystallized by slow cooling from the melt. This is probably due to overestimation of the degree of crystallinity of this sample; indeed, in this work, 1.4 g cm^{-3} is used throughout as crystalline density to compute the degree of crystallinity (ϕ). This is an approximation, increasingly in error as crystallization temperature increased above 573 K or decreases below 473 K.[38] Since the mean crystallization temperature of the slowly-cooled sample is expected to be very high (of the order of 588–593 K based on crystallization kinetics DSC determinations), it is not surprising to observe for this sample important differences between $l_{c,Bragg}$, which requires the knowledge of ϕ, and $l_{c,\gamma}$, which is determined independently of ϕ. The thicknesses determined by the Strobl procedure are on the average 0.96 times the thicknesses determined by the Bragg analysis. This is related to the Strobl analysis giving number averages, and the Bragg analysis weight averages. The agreement between the two analyses suggests that insignificant amounts of interfibrillar amorphous material exist in the samples as compared to interlamellar amorphous polymer.

The evolution of $l_{c,Bragg}$ versus crystallization temperature for isothermally-crystallized samples is displayed in Figure 1B. Data obtained by other workers[3-5] for crystallization times shorter than ~2 h are also shown in this figure. The overall agreement is rather satisfactory, illustrating that the PEEK crystalline core thickness is essentially dependent on crystallization temperature for similar crystallization times, as expected.[49]

The correlation between the thicknesses obtained by the third procedure (direct fit of the paracrystalline model) and the other analysis methods is less satisfactory, although general trends are preserved. This is due to the arbitrary choice of the distribution functions. The only interest of this procedure is to suggest that the distribution function describing the amorphous interlayer thickness could be large.

3.2. Glass Transition. Thermograms and storage and loss moduli of the samples of this study are displayed in Figures 2 and 3 (A and B).

It is obvious that the presence of crystallinity increases strongly the glass transition temperature, while broadening the transition. Starting from the amorphous sample, the appearance of crystallites first increases T_g (nonimpinging spherulites). Then, above ~20% crystallinity (impinging sherulites), the trend is reversed. This behavior corresponds exactly to observations reported for PET. Also,

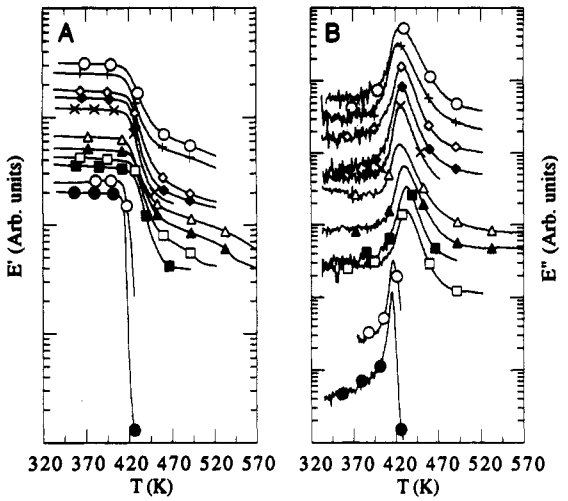

Figure 3. Storage (E', A) and loss (E'', B) moduli of the PEEK samples (1 Hz). The curves have been displaced vertically for clarity. Same symbols as in Figure 2. (All points are not plotted on the figures.)

Table III
Glass Transition Characterization of the PEEK Samples

sample name	$T_{g,DSC}$ (K)	Δc_p (J mol^{-1} K^{-1})	$\phi_{r,am}$	$T_{g,DMA}$ (K)
Q	414.5	~63	0[a]	415.9
G/423	416.0	45.5	0.30	417.3
G/453	439.7	30.9	0.28	433.5
G/493	440.1	24.4	0.35	432.5
G/533	431.8	20.8	0.42	431.2
G/573	427.5	21.0	0.40	425.9
M/393	424.0	29.7	0.32	426.9
M/423	427.0	35.9	0.21	427.9
M/453	438.0	28.5	0.29	428.8
M/573	424.5	18.1	0.43	424.6
M/SC	422.4	43.9	~0	427.4

[a] Hysteresis effects at T_g preclude a precise determination of Δc_p; hence, $\phi_{r,am}$ was considered as zero for this almost fully amorphous sample.

the specific heat jump is decreased in semicrystalline samples, corresponding to very high values of so-called rigid amorphous fractions, $\phi_{r,am}$. For isothermally-crystallized samples, a low-temperature melting endotherm is present roughly 10 K above the crystallization temperature. Corresponding to this endotherm, a weak storage modulus drop can be detected. These phenomena are due to some structural modification of the samples. The exact nature of this modification has been much debated in the recent literature. It has been attributed by some authors[3,4,50,51] to the first trace of a continuous melting–recrystallization process occurring during the heating scan and by others[52,53] to the melting of secondary thin lamellae in between primary thicker lamellae. Another group of authors adopt an intermediate position,[27,37,54] noting that a recrystallization process indeed occurs during DSC scans, while simultaneously supporting,[27] or at least not discarding,[37,54] the existence of two lamellar populations. In all cases, these morphological changes occur at a sufficiently high temperature not to perturb the major part of the glass transition. For some samples, however, the high-temperature side of the glass transition is affected by the partial melting.

A general agreement is found between $T_{g,DSC}$ and $T_{g,DMA}$ (Table III), although the relationship is noisy. Actually, the inherent lower sensitivity of DSC precludes from performing a very precise determination of T_g for the small amounts of matter that were scanned. Moreover, determination of $T_{g,DSC}$ relies upon the choice of two limiting "base lines", the upper of which is somehow difficult to choose, as can be seen from inspection of Figure 2. In this respect, the DMA determination of T_g is much more reliable, being based on a distinct peak value, independent of any "base line" choice.

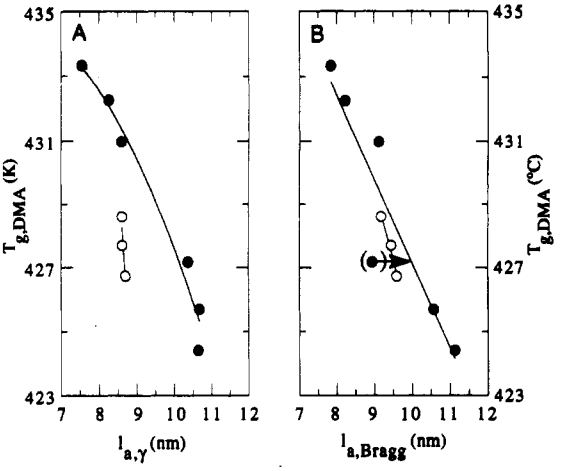

Figure 4. Evolution of the glass transition temperature with the amorphous interlayer thickness (l_a) for semicrystalline samples with impinging spherulites. Filled symbols refer to isothermally-crystallized samples, and open symbols refer to dynamically-crystallized samples. The plot in A is drawn using l_a values obtained from Strobl analysis of correlation functions; the plot in B is drawn using l_a values obtained from Bragg analysis of SAXS patterns. (In B the arrow indicates a probable correction due to poor estimation of the crystallinity of sample M/SC.)

In Figure 4, we present the evolution of $T_{g,DMA}$ with the amorphous layer thickness, $l_{a,\gamma}$ of $l_{a,Bragg}$. The samples have been divided into two categories: those for which most of the crystallization occurred at constant temperature (samples G) or in a small temperature interval (samples M/SC and M/573) and those for which most of the crystallization occurred in truly dynamic conditions (samples M/393, M/423, and M/453). Only samples having impinging sperulites are included in this figure.

A clear relationship exists between the amorphous layer thickness and the glass transition for the (quasi)isothermally-crystallized samples. The dynamically-crystallized samples do not follow the same relationship, although there T_g value decreases also with l_a. This is presumably due to a different distribution of amorphous layer thickness for these samples. Apparently, using weight averages ($l_{a,Bragg}$) instead of number averages ($l_{a,\gamma}$) for the thickness reduces the discrepancy between the two sample categories.

At this stage, one comment should be made relative to the ageing problem described in the Introduction. Since the sample processing was performed while taking care of having similar thermal histories in the glass transition region for each sample and furthermore since the DMA measurements were performed within 1 month of the sample processing, the T_g variations one observes from sample to sample cannot be attributed to differences in the ageing of the samples. Moreover, the T_g variations are far more important than expected from ageing. Finally, $T_{g,DSC}$ and $T_{g,DMA}$ display similar trends, although DSC scans were performed 18 months after sample processing. Clearly, if ageing influences our results, it is in a negligible way.

3.3. Subglass Relaxations. The water influence on the β-relaxation will be first described. Then the role of morphology and ageing will be presented.

3.3.1. Water Influence. The relationship between water content and dielectric permittivity (400 Hz, room temperature) of sample M/573 is displayed in Figure 5. Approximate linear relationships are obtained, the rela-

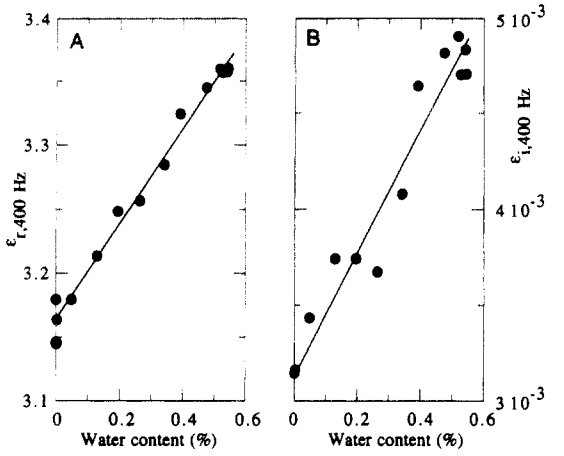

Figure 5. Evolution of the real part (ϵ_r, A) and imaginary part (ϵ_i, B) of the dielectric permittivity of PEEK sample M/573 with water content (weight percent). Data obtained at room temperature on the same sample during progressive sorption and desorption. Test frequency: 400 Hz.

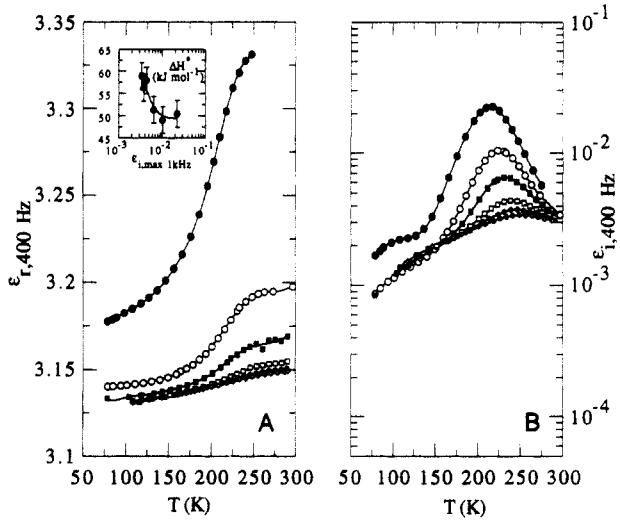

Figure 6. Temperature variation of the real part (ϵ_r, A) and imaginary part (ϵ_i, B) of the dielectric permittivity of PEEK sample M/573 with various water contents (test frequency: 400 Hz): (●) water-saturated sample (~0.55 water weight percent); (○) laboratory atmosphere equilibrated sample; (■, □, ♦, ◇) previous sample after 4, 19, 38, and 64 days of pumping in the cryostat at room temperature. The last sample (◇) can be considered as dry. Inset: Evolution of the activation energy of the M/573 PEEK sample β_w-relaxation as a function of the peak value of the imaginary part of the dielectric permittivity ($\epsilon_{i,max}$ measured at 1 kHz).

tively high dispersion being due to changes in water content between sample weighing and dielectric measurement and during the measurement itself. The same kind of relationship is obtained for other test frequencies and other samples.

The temperature dependence of dielectric permittivity for a sample (M/573) having various water contents is presented in Figure 6. In the remaining sections of this paper, the β-relaxation observed in the presence of water will be called β_w, the term β-relaxation being reserved for the first subglass relaxation of the fully dry PEEK. Apparently, the intensity of the β_w-relaxation is strongly increased by the presence of small water amounts, while its temperature location is shifted toward lower temperatures. The presence of a shoulder at low temperatures is also detected; it corresponds to the γ-relaxation. Its location shifts toward higher temperature upon drying.

The β_w-relaxation activation energies (ΔH^*) were estimated by linear regression between the logarithm of the

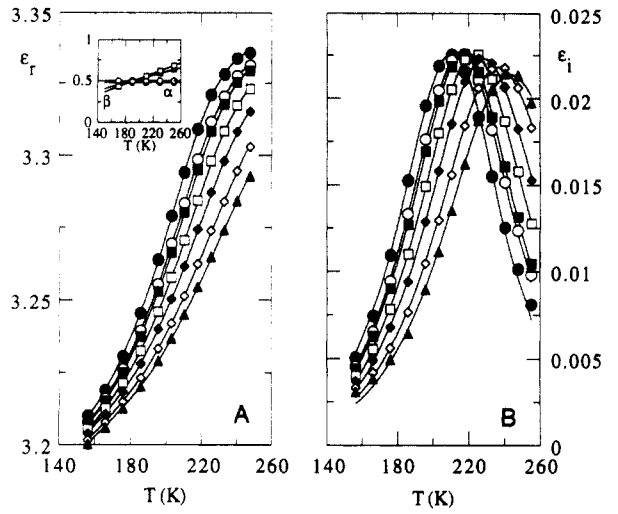

Figure 7. Havriliak-Negami global fit of the β_w-relaxation of water-saturated sample M/573. The dielectric permittivity ($\epsilon_r - j\epsilon_i$) is not drawn above 250 K, due to progressive water desorption during the measurement above this temperature. Test frequency: (●) 200 Hz; (○) 400 Hz; (■) 500 Hz; (□) 1 kHz; (♦) 2 kHz; (◇) 5 kHz; (▲) 10 kHz. Inset: Evolution with temperature of the Havriliak–Negami exponents for water-saturated samples M/573 (filled symbols) and M/293 (open symbols), having well-marked differences in degree of crystallinity. (HN parameters: α, circles; β, squares.)

test frequency and the reciprocal temperature corresponding to the maximum loss ($\epsilon_{i,max}$). In all cases, the Arrhenius relation was found to describe correctly the results. Since $\epsilon_{i,max}$ increases with water content, as can be deduced from inspection of the Figure 6B, a plot of ΔH^* versus $\epsilon_{i,max}$ reflects the evolution of the β_w-activation energy with water content (tending ultimately to the β-activation energy). Such a plot is presented in the inset of Figure 6B. There is some imprecision in the evaluation of activation energies. Indeed, samples having a low water content have a very broad loss peak, whose maximum value is difficult to determine with precision. Samples with higher water contents suffer from some water desorption during the measurement, as revealed by the decrease of ϵ_r at room temperature between the beginning and the end of the experiment. However, the precision is sufficient to observe an increase of the activation energy with a decrease of the water content.

In order to provide a rationale to compare the shape of relaxation curves in the frequency domain as well as in order to obtain values for the dielectric strengths, the sample dielectric permittivities (ϵ^*) were fit in the β_w-region to the phenomenological Havriliak–Negami (HN) equation:[55]

$$\epsilon^* = \epsilon_U + (\epsilon_R - \epsilon_U)(1 + (i\omega\tau_0)^\alpha)^{-\beta} \qquad (2)$$

where U and R refer to unrelaxed values of ϵ_r, ω is the angular frequency, τ_0 is the central dielectric relaxation time, and α and β are two phenomenological shape parameters. ϵ_R, ϵ_U, α, and β were allowed to vary linearly with temperature, while τ_0 was described by an Arrhenius law. Such a procedure has been used by Coburn and Boyd[32] to fit the β-dielectric relaxation of PET. It allows one to take into account the evolution with temperature of the dielectric strength and the relaxation peak broadness, often observed for secondary relaxations.[56]

Experimental data, together with the fit, are shown for the water-saturated M/573 sample in Figure 7. For samples having a high water content, the HN equation was found to describe satisfactorily the experimental data. In these cases, there is no significant difference in the

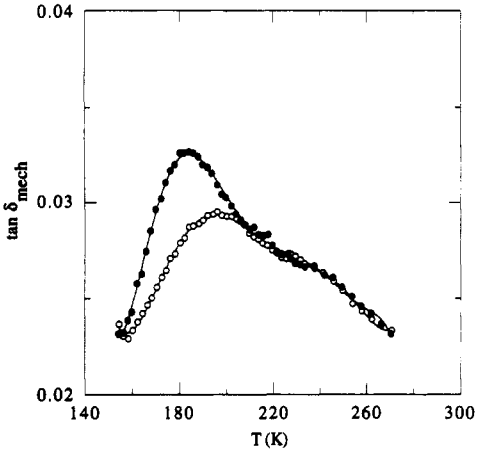

Figure 8. Evolution with water content of the mechanical β-relaxation (loss tangent) of a ~30% crystallinity PEEK sample ((●) water saturated; (○) lower water content). Test frequency: 1 Hz.

relaxation shape (α- and β-parameters) upon changes in sample crystallinity, as can be seen in the inset of Figure 7. Clearly, the β_w-relaxation is independent of sample morphology.

When water content decreases, the HN equation is no more able to represent correctly the β_w-relaxation. This is due to the fact that the β_w-relaxation relative intensity decreases as compared to other mechanisms contributing to the low-temperature losses (see Figure 6). A full description of the dielectric losses requires then the superposition of different HN equations; this involves a definitely too high number of parameters for a meaningful fit to be attempted. It was thus not possible in this work to study the evolution of the β_w-relaxation shape in the frequency domain with changes in water content.

The origin of the β_w-relaxation will be discussed in the discussion section. Before proceeding to the examination of the β-relaxation of fully dry samples, some more comments have to be made. First, exposure of dry PEEK films (2 days of drying at 373 K under primary vacuum) to the laboratory atmosphere for amounts of time as short as 30 min (roughly the time needed to place the sample inside the cryostat) is sufficient for some water to be sorbed in the film. As a result, the dielectric measurements lead to the β_w-relaxation detection instead of the β-relaxation, unless the sample is kept in the cryostat at room temperature under high vacuum for at least 1 week. Struik,[36] studying the mechanical β-relaxation of various polymers, made a similar type of observation for Bisphenol-A polycarbonate (PC) and polysulfone. Thus extreme care has to be taken to measure the β-relaxation of polymers having carbonyl or sulfone groups along the chain. This is not always taken in due consideration. For instance, a brief work on the β-relaxation of various phenylene polymers, including PEEK, has been recently published.[57] Examination of the Arrhenius plot presented for the PEEK dielectric measurements reveals undoubtedly the presence of water in the PEEK sample (the temperatures corresponding to maximum dielectric loss are far lower than in our dry samples, and a too low activation energy is found). Finally, some DMA experiments were performed on PEEK samples having different water contents (Figure 8); these confirmed that the PEEK β-mechanical relaxation is affected by the presence of water, although to a lesser extent than the dielectric relaxation.

3.3.2. Ageing and Morphology Influences on the β-Relaxation (Dry PEEK). The dielectric loss tangents of two PEEK samples, measured at two different ageing

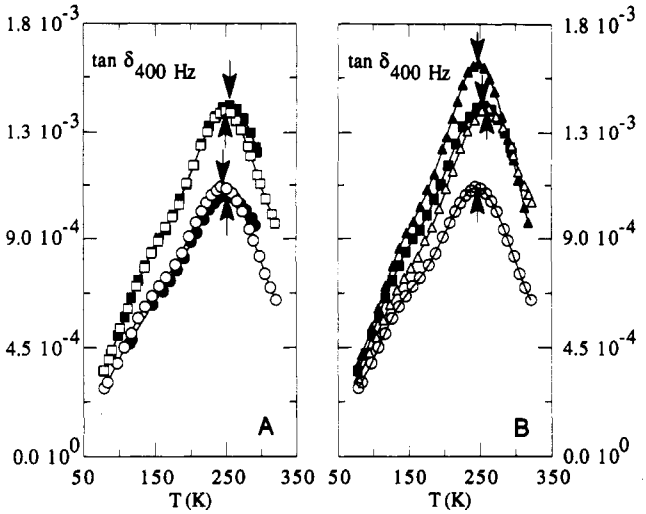

Figure 9. Dielectric loss tangent of dry PEEK in the subglass relaxation range (test frequency: 400 Hz). The arrows indicate the maximum of the β-process. (A) influence of ageing history; (B) influence of semicrystalline morphology and ageing history. Symbols: (▲) sample Q, aged 3 days at 373 K and 7 days at room temperature; (■) sample M/293 aged 5 months at room temperature and 6 days at 373 K; (□) same sample aged 13 months at room temperature and 9 days at 373 K; (△) sample G/453 aged 2 days at 373 K and 60 days at room temperature; (●) sample M/573 aged 11 months at room temperature and 5 weeks at 373 K; (○) same sample aged 19 months at room temperature and 6 weeks at 373 K.

times, are displayed in Figure 9A (tan δ will be preferred to ϵ_i each time different samples have to be plotted together, to get rid of geometrical factor uncertainties). The γ-relaxation and the low-temperature side of the β-relaxation loss peak are unaffected by variations in the sample thermal histories (the small downward shift between the two measurements of sample M/573 is due to a minor experimental problem). However, the high-temperature side of the relaxation is slightly decreased by the increase of ageing. This is consistent with observations made by Struik on other polymers.[36] As a result, the loss maximum location decreases 5–10 K with ageing time. Thus, the claim that β-relaxation peak locations are hardly influenced by thermal histories[36] should be taken in a broad acceptation. It is not clear whether ageing modifies the tail of the glass transition, thereby changing the high-temperature side of the β-relaxation, or directly affects the β-relaxation.

Figure 9B presents the loss tangent (400 Hz) of samples having well-marked differences in morphology. Comparisons should be carefully performed since the ageing histories of these samples are not identical. Sample Q (fully amorphous sample) has been very little aged prior to measurement; however, the loss peak maximum of this sample is located at a lower temperature than the more aged samples M/293 and G/453. Sample M/573 has been very importantly aged but its β-peak location is almost identical to that of the almost unaged sample Q. These complex observations point to the fact that the β-relaxation location results from an interplay between ageing and morphology effects. The stringent requirement to measure fully-dry PEEK samples implies simultaneously that only aged samples can be measured. It is not possible from the present study to dissociate ageing effects, whose rate depends on morphology,[34,35] and direct morphology effects.

Below 200 K, in the γ-relaxation region and in the beginning of the β-relaxation region, the dielectric losses are simply proportional to the amount of amorphous matter in the samples ($1 - \phi$), whatever the ageing history

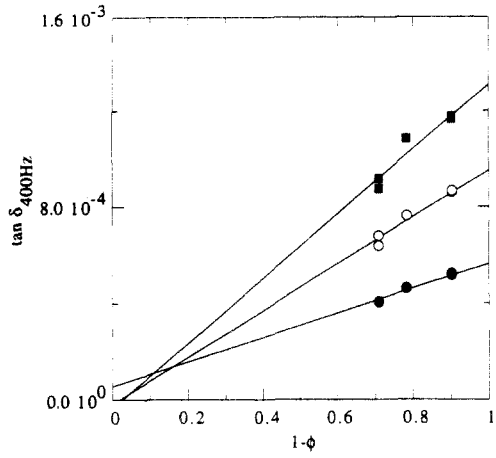

Figure 10. Evolution with amorphous content $(1-\phi)$ of the dry PEEK loss tangent (400 Hz) at selected temperatures in the γ-relaxation region and in the onset of the β-region ($T \leq 200$ K). Symbols: (●) 100 K; (○) 150 K; (■) 200 K.

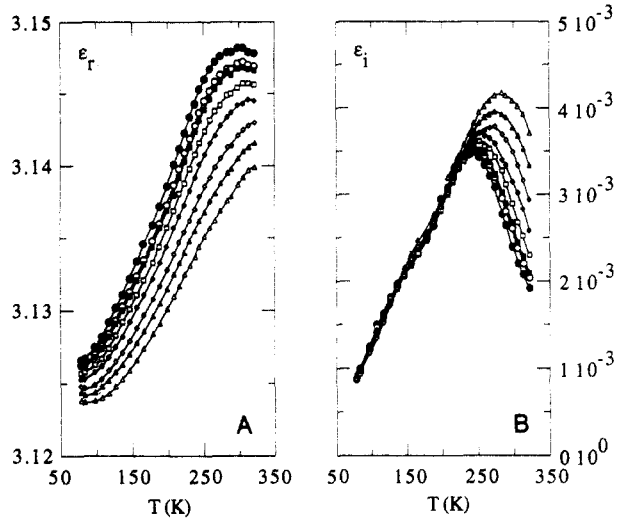

Figure 11. Dependence of the γ- and β-relaxations of dry sample M/573 on temperature and frequency. Test frequency: (●) 200 Hz; (○) 400 Hz; (■) 500 Hz; (□) 1 kHz; (♦) 2 kHz; (◇) 5 kHz; (▲) 10 kHz; (△) 20 kHz.

or sample lamellar morphology (Figure 10). However, above 200 K, this relation does not hold anymore. Clearly, lamellar morphology and/or ageing influences the β-relaxation location.

Figure 11 presents the dielectric permittivity of sample M/573 as a function of temperature for various frequencies. Identical behaviors are obtained for other samples, with some differences in the intensity and the location of the β-relaxation as described above. A striking feature of the PEEK dielectric losses is the very weak frequency dependence one observes below ~220 K in the γ-relaxation region and in the beginning of the β-relaxation region (for frequencies ranging from 2×10^2 to 2×10^4 Hz). More exactly, the frequency dependence is beyond the ϵ_i resolution of the measuring system (~2%). The temperature dependence of ϵ_i is much greater than its frequency dependence. The existence of temperature-dependent dielectric losses, having only a weak frequency dependence, has been documented in the literature;[58] however, their actual origin is not yet well established. Activation energies computed from the frequency dependence of the β-loss peak maximum were found to be 61.5 ± 3 kJ mol^{-1}, with no significant difference between the various samples.

4. Discussion

4.1. The γ-Region (77–200 K). The possible motions in this temperature range are very restricted; phenyl group flipping will be demonstrated below to occur only at higher temperatures. Consequently, the molecular motions occurring in the γ-range must be of smaller amplitude; since they are dielectrically active, they probably consist in restricted wagging of the polar bridges without correlated intra- and interchain motions. The highly localized nature of these motions implies that they are directly dependent on local potentials resulting from chain packing and neighboring phenyl tilt angles. The atomic-scale disorder of the amorphous regions is expected to give rise to a very broad spectrum of local potentials and thus to a very broad distribution of activation energies; this results in a small frequency dependence of the dielectric loss, as observed. The strong temperature dependence of the γ-relaxation (as compared to its frequency dependence) could be due to a progressive increase of the γ-wagging amplitude, leading ultimately to the β-relaxation more complex motion. Indeed, the onset of the β-relaxation displays features similar to those of the γ-relaxation, namely a small dependence on frequency, insensitivity to ageing, and details of morphology. Moreover, as can be observed in Figure 11, there is no clear-cut separation between the two low-temperature relaxation processes, suggesting the progressive transformation of the γ-motions into β-motions.

4.2. The β-Relaxation. A major phenomenon able to explain the transformation of the localized γ-wagging into a more complex β-motion is the appearance of phenyl flips occurring at frequencies comparable to the testing frequencies. A recent solid-state ^{13}C NMR study of PEEK[59] has revealed that a fraction of the phenyl rings (between 10 and 40% following crystallinity) undergoes 180° flips superimposed on small-amplitude phenyl oscillations and wiggles at room temperature. The average frequency of these flips, oscillations, and wiggles was estimated to be of the order of 100 kHz to 1 MHz at room temperature for samples of uncontrolled water content. From an Arrhenius extrapolation of measurements performed on three samples measured without any prior drying procedure, the average frequency of the dielectric β_w relaxation is found to be 160–210 kHz at room temperature, in good agreement with the previous NMR estimation. A similar correspondence between the temperature/frequency dependence of the secondary transition and the frequency of ring flipping has been found for Bisphenol-A polycarbonate (PCBPA).[60]

Thus, the onset of β-motions is dictated by the onset of phenyl flips. The β-motions are not restricted to phenyl flips since these are not per se dielectrically or mechanically active. But the coupling of these flips with the γ-wagging provides room to the appearance, of a larger-scale motion involving the polar bridges. When phenyls are blocked, steric hindrances between neighboring phenyls during conformational changes drastically reduce the available range of chain conformations. The relief of these hindrances to conformational changes is probably the main reason which explains the appearance of the β-motion as soon as phenyl flips occur. The exact molecular motion associated with the β-relaxation cannot be detailed on the basis of our experiments. However, some information on this motion will be given below. This requires first the consideration of the effects water has on the β-relaxation.

4.2.1. Water Influence. The β_w-relaxation is not simply due to uncorrelated motions of water inside the PEEK matrix. In such a hypothesis, it is possible to compute the relaxation strength due to the water molecules by using

the Fröhlich-Kirkwood theory:[61]

$$\epsilon_R - \epsilon_U = \frac{3\epsilon_R}{2\epsilon_R + \epsilon_U} \frac{N}{3kT\epsilon_0} \left(\frac{\epsilon_U + 2}{3}\right)^2 g\mu_0^2 \qquad (3)$$

with ϵ_R and ϵ_U the relaxed and unrelaxed value of ϵ_r, N the density of water molecules (having μ_0 as dipole moment in vacuum), g the correlation factor, and ϵ_0 the vacuum permittivity.[62] For the water-saturated sample M/293 (0.77 wt % of water for ~10% crystallinity, thus ~605 mol·m^{-3} water in the amorphous regions), using parameters derived from the HN fit of the β_w-relaxation ($\epsilon_U = 3.22$ at 250 K and $(\epsilon_R - \epsilon_U) \ll \epsilon_U$), and taking $\mu_0 = 6.08 \times 10^{-30}$ C·m (i.e., 1.82 D), one finds that $(\epsilon_R - \epsilon_U)$ should be 0.44 g at 250 K. For the low water concentrations of the water-saturated PEEK samples, there is on the average only one water molecule per 2.75 nm^3; there is thus no orientational correlation between water molecules and $g = 1$. The value obtained from the NH fit is $(\epsilon_R - \epsilon_U) = 0.175$.

One could wonder if the discrepancy between the expected value and the measured value is not due to some water clustering. In this case, the correlation factor should be different from unity. Actually, g is expected to increase above unity, as correlations between water dipoles should be similar to that found in water,[61] and the discrepancy sould be even worse. Also, the discrepancy is not due to water desorption during the sample mounting in the cryostat: from results on water diffusion in PEEK published by others,[63] we estimated that an upper bound to the water loss during sample mounting is ~25% (leading to $(\epsilon_R - \epsilon_U) \approx 0.34$ g). Thus the conclusion follows that the discrepancy arises from the choice of an incorrect model: the dielectric β_w-losses are not due to uncorrelated motions of water in PEEK.

In other words, the water motions are restricted due to interaction with neighboring PEEK chains (they are correlated to the local environment). This is in agreement with previous infrared spectroscopy results showing that water is bonded to PEEK.[64] Moreover, these water motions are coupled to some motion of neighboring PEEK chain segments, since water affects the PEEK mechanical relaxation. Furthermore, the β_w-relaxation tends smoothly to the dry PEEK β-relaxation upon water desorption (Figure 6). Clearly, the dielectric relaxation cannot be described as the sum of two independent processes, the first being due to water motions, and the second to PEEK chain β-motions. Actually, water acts as a β-plasticizer: increasing the water content decreases the β-relaxation temperature location, while the activation energy decreases.

Thus, the β_w-relaxation involves a cooperative motion of a PEEK segment and a water molecule, the PEEK segment motion being similar to the β-motion occurring in dry PEEK. The water presence allows an easier PEEK segment motion, as revealed by the lower activation energies required. From water sorption studies,[63] it was concluded that there is some distortion in the amorphous chain packing in the vicinity of a sorbed water molecule. The β-motion of a PEEK segment will be easier in the neighborhood of a water molecule, since this molecule will accommodate with the motion of the PEEK segment more easily than the usual chain environment, in a kind of positional exchange. Thus, activation energy is reduced, and the intensity of the relaxation is increased, probably not only due to the supplementary motion of the water dipole moment but also due to an increase of the number of PEEK chain segments able to undergo the β-motion.

4.2.2. Dry PEEK β-Motions. It was demonstrated above that the PEEK β-motion is controlled by the onset of phenyl flips. Now a question to be addressed is whether the phenyl flipping rate is controlled by intramolecular energy barriers or by external barriers. C-INDO[65] and ab initio[66-68] computations on diphenyl ether and benzophenone have shown that the energy internal barriers to phenyl rotation are small in these PEEK model compounds (8.8,[65] 5.4,[67] or 7.1[68] kJ mol^{-1} for benzophenone; 1.3,[65] 0.7,[66] or 0.4[68] kJ mol^{-1} for diphenyl ether), provided the rotations of the two phenyls are properly correlated. However, when one phenyl is blocked in its equilibrium angular position, the energy barrier for rotation of the other phenyl increases[65,66] around 40–50 kJ mol^{-1}. Thus, in dilute solution at room temperature, PEEK phenyl groups will undergo easy rotational motions. This is supported by the observation[69] that PEEK in solution at 303 K behaves like a freely rotating chain with approximately 120° valence angles: the phenyl groups virtually can be considered as long chemical bonds, connecting together the ketone and ether bridges. The internal barriers to phenyl rotation are easily crossed in such conditions, in accordance with theoretical predictions. Hence, the isolated PEEK chain is not intrinsically rigid at room temperature.

However, in the condensed state, only a restricted fraction of the PEEK phenyls are undergoing π-flips at room temperature (10–40% following crystallinity).[59] This implies that the others are blocked due to environmental constraints resulting from the close packing. The blocking of these phenyls by external energy barriers results in turn in a dramatic increase of the internal barriers to be crossed by the flipping phenyls. This explains the high value of the β-relaxation activation energy. Thus, the β-motion is essentially controlled by intermolecular interactions, partly relayed from one phenyl to the next by intramolecular barriers. The external control of the relaxation rate is supported by two supplementary observations: (1) the β-relaxation is affected by ageing or details of the semicrystalline morphology and thus changes in the relaxing segment environment; (2) the β-relaxation is significantly affected by the presence of water molecules which perturb the environment of the relaxing segment.

As pointed out above, the β-relaxation of PCBPA is also controlled by the onset of phenyl flips. It is probable that the β-motions of both polymers bear some similarity, since the β-motions of PEEK are mostly determined by external hindrances due to the chain packing in the amorphous state, the same holding for PCBPA.[70] Experimental studies performed on block copolymers (with miscible blocks) led Jho and Yee[70] to the conclusion that the subglass relaxation of PCBPA requires both inter- and intrachain cooperations to occur. The same conclusion was obtained when the so-called coupling model[71] was used to interpret the β-relaxation of pure PCBPA. It has thus to be expected that the β-motion of PEEK requires also some cooperative motions of the environment of the relaxing segment, although this cannot be deduced directly from our measurements. It is probable that these considerations hold for many other aromatic polymers whose secondary transitions bear similarity with PEEK in some respects (PET,[31] poly(phenylene sulfide),[72] various poly(aryl ether)s and poly(aryl sulfone)s,[73-75] etc.)

4.3. Glass Transition. The cooperative nature of the large-scale segmental motions whose onset defines the glass transition has often been theoretically postulated; examples are thermodynamic[76] or kinetic[77,78] entropy-based glass transition theories, coupling model,[71] and many other models.[79-86] Due to this cooperative nature, any modification in the number of accessible chain conformations will affect the T_g of a given polymer: a decrease of this

number is associated with an increase of the glass transition temperature. For instance, the Gibbs–Di Marzio theory[76] states that, due to the loss of freedom resulting from a decrease of the number of accessible conformations, the large-scale segmental motions require a higher thermal energy to be initiated.

In the semicrystalline morpholgy, the connections of amorphous segments to crystallites,[87] the stretching[88,89] or squeezing[90] of polymer coils in the amorphous regions, and the trapping of entanglements in these regions[90,91] contribute to restrict the region of phase space which can be explored by a set of chains of an amorphous region, as compared to the same chains without boundary conditions imposed by the crystallites' presence. As l_a increases with T_c, one may expect that the relative influence of these boundary conditions will decrease, resulting in the observed decrease of T_g with l_a.

If we assume that the amorphous regions are in equilibrium given the boundary conditions imposed by the crystallization, the T_g variations can be thermodynamically related to variations of the configurational entropy (S_c) of the amorphous regions. Attempts to introduce in the crystallization free energy terms arising from the entropy decrease in the amorphous regions as crystallization proceeds can be found in the literature.[88-91] In these models, the growth of the crystalline lamellae,[88,89] or more interestingly the interlamellar distance,[90] are controlled by the entropy decrease in the amorphous regions upon crystallization. In the frame of such models, the relationship between T_g and l_a is clearly expected from their common dependency on S_c.

4.4. The PEEK Amorphous Interlayer. In the Introduction, mention was made that the structure of semicrystalline polymers has to be described with a three-region model, including the crystalline phase, the amorphous liquid-like phase, and the interphase region. The interphase region is defined as a spatial region in which an experimental parameter $P(r)$ progressively varies between the crystal value and the bulk amorphous phase value. Unfortunately, with such a definition, the interphase spatial extent depends on the parameter P selected to probe it. For instance, one could use the local average segment orientation relative to the crystal/amorphous interface,[10] the local amount of a given chain conformation,[12-14] the local density,[15-17] the local value of the relaxation time associated with a given motion,[18-21] etc. To each parameter could correspond a different estimation of the interphase thickness.

Highly-localized molecular motions, like the PEEK γ-motions, are sensitive to local potential barriers. Since they are not cooperative, the relaxation curve in the frequency domain reflects a distribution of relaxation times originating from a wide variety of local environments. One would expect a shifting of this curve toward longer relaxation times for the denser interphase regions, similarly to what is reported for the effect of pressure on local secondary relaxation.[56] However, the very small dependence on frequency of the PEEK γ-losses and the superposition of the β-relaxation on the γ-relaxation above $\sim$200 K prevent the detection of this phenomenon in our frequency range.

For the long-range cooperative motions occurring near T_g, it is no longer valid to consider the relaxation curves as reflecting a distribution of local relaxation times.[71,80] However, for a sample having large amounts of interspherulitic amorphous regions (G/423), the loss modulus curve can be considered as the superposition of a loss peak identical to that of a pure amorphous sample, plus a loss peak originating from intraspherulitic amorphous regions. This is shown in Figure 12, where the result of the deconvolution of the loss modulus of this sample by the loss modulus of the pure amorphous sample is presented, assuming

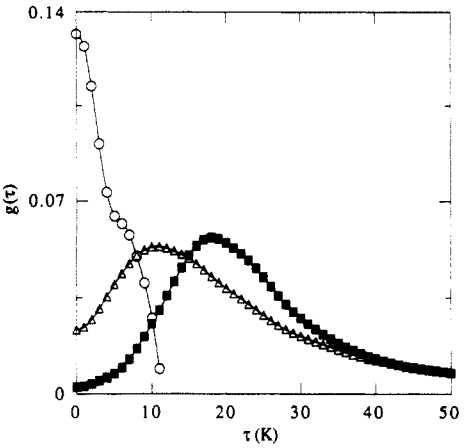

Figure 12. Typical examples of the convolution function $g(\tau)$ defined in eq 3. Symbols: (○) G/423; (■) G/453; (△) G/573.

$$E''(T) = \int_{\tau=0}^{\infty} E''_{am}(T-\tau)g(\tau)\,d\tau \qquad (4)$$

The presence in the convolution function $g(\tau)$ of a sharp peak located at the origin testifies for the presence of significant amounts of amorphous matter behaving like the pure amorphous PEEK. This origin peak is not observed for samples wherein spherulites impinge, as shown in Figure 12. This means that inside spherulites there are no amorphous regions large enough (as compared to the size of the cooperative motions occurring at T_g) to be considered as truly liquid-like. Or, stated otherwise, if the amorphous interlayers are probed with the large-range α-motions, they must be considered as consisting essentially of interphase regions. Of course, this is a conclusion which would not be obtained by using more localized motions, for which the influence of the crystallite boundaries would vanish for shorter distances. It is related to a particular choice of the parameter P used to characterize the interphase.

It has been stated in the literature[28,92,93] that the so-called rigid amorphous fraction $\phi_{r,am}$ is located in the crystalline/amorphous interphase. If we consider the entropy of amorphous regions as arising in part from a configurational term S_c independent of other entropy terms (vibrational etc.), the difference between the liquid and glass specific heats (for 1 g of amorphous region) is

$$c_{p,liq} - c_{p,glass} = T\left.\frac{d(S_{liq} - S_{glass})}{dT}\right|_p \simeq T\left.\frac{dS_{c,liq}}{dT}\right|_p \qquad (5)$$

Hence, for the semicrystalline polymer, the specific heat jump at T_g is

$$\Delta c_p(T_g) = (1 - \psi - \psi^*_{am})T_g\left.\frac{dS_{c,liq}}{dT}\right|_{p,T_g} \qquad (6)$$

where $S_{c,liq}$ is defined per gram of amorphous material and c_p per gram of semicrystalline material and ψ^*_{am} is the weight fraction of amorphous matter not able to participate in the relaxation (tight folds, extended tie molecules, and so on). For PEEK, it is clear that the so-called rigid amorphous fraction $\phi_{r,am}$, as defined by eq 1, is not equal to ψ^*_{am}, since $S_{c,liq}$ depends on the morphology of semicrystalline PEEK as attested to by the large T_g variations. In this case, it is difficult to find a physical meaning for $\phi_{r,am}$, but it should not be equated to a volume

fraction of amorphous regions not participating in the glass transition due to "immobilization" by crystallites. Actually, the term "rigid amorphous fraction" is somewhat misleading. It includes the true rigid amorphous fraction (ψ^*_{am}) as well as contributions due to differences in the temperature derivative of the entropy of amorphous regions participating in the relaxation. Hence, there are no reasons to consider it to be proportional to the volume of the crystalline/amorphous interphase. It is located in regions where configurational entropy differs from that of the pure amorphous polymer, i.e., in almost the whole amorphous interlayer in the case of semicrystalline PEEK. Similar comments should be valid for other semicrystalline polymers having para-aromatic groups in their main chain and having strong dependences of T_g with crystallinity (PET,[29-32] various aromatic polycarbonates,[19] poly(phenylene sulfide)[94]), but are unassailable for polymers like polypropylene and isotactic polystyrene, whose T_g's are almost morphology independent.[19,95]

5. Conclusions

In this paper, the relation between the PEEK subglass relaxations and glass transition and its semicrystalline morphology has been studied by various techniques. The major observations are as follows:

1. Interpretations of PEEK SAXS patterns using either a simple Bragg analysis or the Strobl correlation function analysis give similar results. This suggests that insigificant amounts of interfibrillar amorphous material exist in samples with impinging spherulites, as compared to interlamellar amorphous polymer.

2. Two subglass relaxations have been observed by dielectric spectroscopy and tentatively interpreted in terms of molecular motions. A highly-localized motion (γ-wagging) was shown to occur in the amorphous regions and to be independent of the morphological details of the semicrystalline arrangement. The combination of phenyl flips with γ-wagging results in the appearance of a larger-scale β-motion at higher temperatures. The barriers controlling the β-motion are determined by intermolecular interactions, relayed by phenyl intramolecular rotational barriers. Variations of the relaxing moiety environment with water content, ageing history, or sample morphology consequently affect the location of the β-loss peak.

3. The PEEK glass transition has been shown to be extremely sensitive to the semicrystalline morphology. A correlation between the amorphous interlayer thickness and the glass transition has been found. It is suggested that both parameters, T_g and l_a, are dependent on the configurational entropy reduction experienced by the amorphous regions while crystallization proceeds, lower crystallization temperatures corresponding to larger entropy reductions, smaller l_a's, and higher T_g's. The entropy changes in the amorphous regions are also illustrated by specific heat jump perturbations (the so-called "rigid amorphous fraction").

These observations contribute to further our knowledge of the PEEK semicrystalline morphology. An interesting observation is that almost no true liquid-like amorphous phase exists in semicrystalline PEEK samples with impinging spherulites, if the amorphous regions are probed with the long-range α-motions. This clearly brings important consequences on the description of PEEK crystallization, since the properties of the PEEK amorphous regions are depending on the crystallite formation. This should be taken into account in a proper crystallization theory.

In various instances, the similarity between the relaxation behavior of PEEK and various other para-aromatic polymers has been pointed out (water influence on the β-relaxation, coincidence between the onset of phenyl flips and β-motions, influence of crystallinity on T_g). The relaxation behavior of this important polymer class could be probably rationalized in a general picture.

Acknowledgment. It is a pleasure to acknowledge Prof. H. Reynaers for access to the SAXS facilities of the Laboratory for Macromolecular Structural Chemistry of the Katholieke Universiteit van Leuven and for fruitful discussions concerning SAXS interpretation. We are grateful to M. Peeters and Dr. R. Scherrenberg for their help in obtaining the SAXS patterns. The authors are indebted to M. Lambricht for his continuous attention and encouraging remarks during the development of the dielectric system. The PEEK powder used in this study was kindly supplied by Dr. P. T. McGrail of I.C.I., Wilton, U.K. This work was supported by the Belgian National Fund for Scientific Research.

References and Notes

(1) Nguyen, H. X.; Ishida, H. *Polym. Compos.* **1987**, *8*, 57.
(2) Jonas, A.; Legras, R. *Polymer* **1991**, *32*, 2691.
(3) Blundell, D. J.; Osborn, B. N. *Polymer* **1983**, *24*, 953.
(4) Blundell, D. J. *Polymer* **1987**, *28*, 2248.
(5) Cebe, P.; Chung, S. Y.; Hong, S.-D. *J. Appl. Polym. Sci.* **1987**, *33*, 487.
(6) Cebe, P. *J. Mater. Sci.* **1988**, *23*, 3721.
(7) Mansfield, M. L. *Macromolecules* **1983**, *16*, 914.
(8) Marqusee, J. A.; Dill, K. A. *Macromolecules* **1986**, *19*, 2420.
(9) Marqusee, J. A. *Macromolecules* **1989**, *22*, 472.
(10) Kumar, S. K.; Yoon, D. Y. *Macromolecules* **1989**, *22*, 3458.
(11) See *Faraday Discuss. Chem. Soc.* **1979**, *68*.
(12) Strobl, G. R.; Hagedorn, W. *J. Polym. Sci., Polym. Phys. Ed.* **1978**, *16*, 1181.
(13) Glotin, M.; Mandelkern, L. *Colloid Polym. Sci.* **1982**, *260*, 182.
(14) Mandelkern, L.; Alamo, R. G.; Kennedy, M. A. *Macromolecules* **1990**, *23*, 4721.
(15) Hahn, B.; Wendorff, J.; Yoon, D. Y. *Macromolecules* **1985**, *18*, 718.
(16) Hahn, B. R.; Herrmann-Schönherr, O.; Wendorff, J. H. *Polymer* **1987**, *28*, 201.
(17) Russell, T. P.; Ito, H.; Wignall, G. D. *Macromolecules* **1988**, *21*, 1703.
(18) See, e.g.: McBrierty, V. J. *Faraday Discuss. Chem. Soc.* **1979**, *68*, 78. Kitamaru, R.; Horri, F.; Murayama, K. *Macromolecules* **1986**, *19*, 636. Monnerie, L. In *Molecular Dynamics and Relaxation Phenomena in Glasses*; Dorfmüller, Th., Williams, G., Eds.; Springer-Verlag: Berlin, 1987; p 125.
(19) McCrum, N. G.; Read, B. E.; Williams, G. *Anelastic and Dielectric Effects in Polymeric Solids*; John Wiley & Sons: London, 1967.
(20) Williams, G. In *Static and Dynamic Properties of the Polymeric Solid State (Proc. NATO Adv. Study Inst., Glasgow, 1981)*; Pethrick, R. A., Richards, R. W., Eds.; D. Reidel: Dordrecht, 1981; p 213.
(21) Boyd, R. H. *Polymer* **1985**, *26*, 323.
(22) Struik, L. C. E. *Physical Aging in Amorphous Polymers and Other Materials*; Elsevier: Amsterdam, 1978. Struik, L. C. E. *Polymer* **1987**, *28*, 1521, 1534; **1989**, *30*, 799, 815.
(23) Use of the term "phase" for the interfacial transition region (interphase) is inappropriate; indeed, the properties of this spatial region are not uniquely determined by thermodynamic variables such as pressure, temperature, and composition.
(24) Sasuga, T.; Hagiwara, M. *Polymer* **1985**, *26*, 501.
(25) The relaxation nomenclature used in this paper differs from that used by Sasuga and Hagiwara (SH).[24] The onset of segmental motions associated with glass transition is denoted by α in the present paper (SH: β), while the first subglass relaxation is denoted by β (SH: γ). The γ-relaxation of the present paper occurs below the temperature range scanned by SH. The differences between the two nomenclatures is due to the fact that SH denoted the mechanical loss peak corresponding to the cold crystallization of amorphous PEEK by α'. However, this peak cannot be considered as a relaxation in the usual meaning, being associated with irreversible morphological changes.
(26) Ahlborn, K. *Cryogenics* **1988**, *28*, 234.

(27) Cheng, S. Z. D.; Cao, M.-Y.; Wunderlich, B. *Macromolecules* **1986**, *19*, 1868.
(28) Huo, P.; Cebe, P. *Macromolecules* **1992**, *25*, 902.
(29) Reddish, W. *Trans. Faraday Soc.* **1950**, *46*, 459.
(30) Ishida, Y.; Yamafuji, K.; Ito, H.; Takayanagi, M. *Kolloid Z.-Z. Polym.* **1962**, *184*, 97.
(31) Illers, K. H.; Breuer, H. *J. Colloid Sci.* **1963**, *18*, 1.
(32) Coburn, J. C.; Boyd, R. H. *Macromolecules* **1986**, *19*, 2238.
(33) Kemmish, D. J.; Hay, J. N. *Polymer* **1985**, *26*, 905.
(34) Ogale, A. A. Ph.D. Dissertation, University of Delaware, 1986.
(35) D'Amore, A.; Cocchini, F.; Pompo, A.; Apicella, A.; Nicolais, L. *J. Appl. Polym. Sci.* **1990**, *39*, 1163.
(36) Struik, L. C. E. *Polymer* **1987**, *28*, 57.
(37) Jonas, A.; Legras, R.; Issi, J.-P. *Polymer* **1991**, *32*, 3365.
(38) Jonas, A.; Legras, R. In *Advanced Thermoplastics and Their Composites*; Kausch, H. H., Ed.; Carl Hanser: München, Chapter 3, in press.
(39) Jonas, A.; Legras, R.; Scherrenberg, R.; Reynaers, H., submitted.
(40) Between 50 K and T_g, polymer specific heats are largely independent of crystallinity. It is thus customary to use the term "solid" specific heat to designate the polymer specific heat in this temperature region.
(41) Cheng, S. Z. D.; Lim, S.; Judovits, L. H.; Wunderlich, B. *Polymer* **1987**, *28*, 10.
(42) Cheng, S. Z. D.; Wunderlich, B. *J. Polym. Sci., Part B: Polym. Phys. Ed.* **1986**, *24*, 1755.
(43) For details on the concept of rigid amorphous fraction, refer to papers of Wunderlich et al.: Grebowicz, J.; Lau, S.-F.; Wunderlich, B. *J. Polym. Sci., Polym. Symp*, **1984**, *71*, 19. Suzuki, H.; Grebowicz, J.; Wunderlich, B. *Makromol. Chem.* **1985**, *186*, 1109. Cheng, S. Z. D.; Cao, M.-Y.; Wunderlich, B. *Macromolecules* **1986**, *19*, 1868. Cheng, S. Z. D.; Wunderlich, B. *Macromolecules* **1987**, *20*, 1630. Cheng, S. Z. D. *J. Appl. Polym. Sci., Appl. Polym. Symp.* **1989**, *43*, 315.
(44) Jonas, A. Ph.D. Thesis, Université Catholique de Louvain, 1992.
(45) Lee, Y. D.; Phillips, P. J.; Lin, J. S. *J. Polym. Sci., Part B: Polym. Phys. Ed.* **1991**, *29*, 1235.
(46) Balta-Calleja, F. J.; Vonk, C. G. *X-Ray Scattering of Synthetic Polymers*; Elsevier: Amsterdam, 1989.
(47) Strobl, G. R.; Schneider, M. *J. Polym. Sci., Polym. Phys. Ed.* **1980**, *18*, 1343.
(48) Crist, B. *J. Polym. Sci., Polym. Phys. Ed.* **1973**, *11*, 635, 1023.
(49) Wunderlich, B. *Macromolecular Physics. Crystal Nucleation, Growth, Annealing*; Acadmic Press: New York, 1976; Vol. 2.
(50) Lee, Y.; Porter, R. S. *Macromolecules* **1987**, *20*, 1336.
(51) Lee, Y.; Porter, R. S.; Lin, J. S. *Macromolecules* **1989**, *22*, 1756.
(52) Bassett, D. C.; Olley, R. H.; Al Raheil, I. A. M. *Polymer* **1988**, *29*, 1745.
(53) Cebe, P.; Hong, S. D. *Polymer* **1986**, *27*, 1183.
(54) Crevecoeur, G.; Groeninckx, G. *Macromolecules* **1991**, *24*, 1190.
(55) Havriliak, S.; Negami, S. *Polymer* **1967**, *8*, 161.
(56) Johari, G. P. In *Molecular Dynamics and Relaxation Phenomena in Glasses*; Th., Dorfmüller, G., Williams, Eds.; Springer-Verlag: Berlin, 1987; p 90.
(57) Starkweather, H. W.; Avakian, P. *Macromolecules* **1989**, *22*, 4060.
(58) Jonscher, A. K. In *Physics of Thin Films*; Francombe, M. H., Ed.; Academic Press: London, 1980; Vol. 11, p 205.
(59) Poliks, M. D.; Schaefer, J. *Macromolecules* **1990**, *23*, 3426.
(60) Roy, A. K.; Jones, A. A.; Inglefield, P. T. *Macromolecules* **1986**, *19*, 1356.
(61) Fröhlich, H. *Theory of Dielectrics, Dielectric Constant and Dielectric Losses*; Oxford University Press: Oxford, 1949.
(62) This equation is given in S.I. units, instead of Gaussian units as usual.
(63) Grayson, M. A.; Wolf, C. J. *J. Polym. Sci., Part B: Polym. Phys.* **1987**, *25*, 31.
(64) Daoust, D.; Devaux, J.; Godard, P.; Jonas, A.; Legras, R. In *Advanced Thermoplastics and Their Composites*; Kausch, H. H., Ed.; Carl Hanser: München, Chapter 1, in press.
(65) Baraldi, I.; Gallinella, E.; Momicchioli, F. *J. Chim. Phys. Phys.-Chim. Biol.* **1986**, *83*, 653.
(66) Schaefer, T.; Penner, G. H.; Takeuchi, C.; Tseki, P. *Can. J. Chem.* **1988**, *66*, 1647.
(67) Abraham, R. J.; Haworth, I. S. *J. Chem. Soc., Perkin Trans. 2*, **1988**, 1429.
(68) Kendrick, J. *J. Chem. Soc., Faraday Trans.* **1990**, *86*, 3995.
(69) Roovers, J.; Cooney, J. D.; Toporowski, P. M. *Macromolecules* **1990**, *23*, 1611.
(70) Jho, J. Y.; Yee, A. F. *Macromolecules* **1991**, *24*, 1905.
(71) For a review of the coupling theory of K. L. Ngai and co-workers, see: Ngai, K. L. In *Basic Features of the Glassy State* (Proceedings of the Second International Workshop on Non-crystalline Solids, San Sebastian, July 1989) Colmonero, J., Alegria, A., Eds.; World Scientific: Singapore, 1990; p 265. Ngai, K. L.; Rendell, R. W.; Rajagopal, A. K.; Teitler, S. In *Dynamic Aspects of Structural Change in Liquids and Glasses* (*Ann. N.Y. Acad. Sci.* Vol. 484); Angell, C. A., Goldstein, M., Eds.; The New York Academy of Sciences: New York, 1986; p 150. Application of the theory to the secondary relaxation of PCBPA can be found in: Ngai, K. L.; Rendell, R. W.; Yee, A. F. *Macromolecules* **1988**, *21*, 3396. Ngai, K. L.; Rendell, R. W.; Yee, A. F.; Plazek, D. J. *Macromolecules* **1991**, *24*, 61.
(72) Henrichs, P. M.; Nicely, V. A.; Fagerburg, D. R. *Macromolecules* **1991**, *24*, 4033.
(73) Robeson, L. M.; Farnham, A. G.; McGrath, J. E. In *Molecular Basis of Transitions and Relaxations*; Meier, D. J., Ed.; Gordon and Breach: London, 1978; p 405.
(74) Allen, G.; McAinsh, J.; Jeffs, G. M. *Polymer* **1971**, *12*, 85.
(75) Johnson, G. E.; Bair, H. E.; Matsuoka, S.; Anderson, E. W.; Scott, J. E. In *Water in Polymers*; Rowland, S. P., Ed.; American Chemical Society: Washington, DC, 1980; p 451.
(76) Gibbs, J. H.; Di Marzio, E. A. *J. Chem. Phys.* **1958**, *28*, 373.
(77) Adam, G.; Gibbs, J. H. *J. Chem. Phys.* **1965**, *43*, 139.
(78) Matsuoka, S.; Quan, X. *Macromolecules* **1991**, *24*, 2770.
(79) Donth, E. *J. Non-Cryst. Solids* **1982**, *53*, 325.
(80) Jonscher, A. K. *Dielectric Relaxation in Solids*; Chelsea Dielectrics Press: London, 1983.
(81) Dissado, L. A.; Hill, R. M. *Proc. R. Soc. London* **1983**, *A390*, 131.
(82) Skinner, J. L. *J. Chem. Phys.* **1983**, *79*, 1955.
(83) Owen, A. J.; Bonart, R. *Polymer* **1985**, *26*, 1034.
(84) Schönhals, A.; Schlosser, E. *Colloid Polym. Sci.* **1989**, *267*, 125.
(85) Adachi, K. *Macromolecules* **1990**, *23*, 1816.
(86) Etienne, S.; Cavaillé, J. Y.; Perez, J. *J. Non-Cryst. Solids* **1991**, *131–133*, 66.
(87) Zachmann, H. G. *Kolloid Z.-Z. Polym.* **1969**, *231*, 504.
(88) Roe, R.-J.; Smith, K. J., Krigbaum, W. R. *J. Chem. Phys.* **1961**, *35*, 1306.
(89) Krigbaum, W. R.; Uematsu, I. *J. Polym. Sci., Part A* **1965**, *3*, 2915.
(90) Robelin-Souffaché, E.; Rault, J. *Macromolecules* **1989**, *22*, 3581.
(91) Mansfield, M. L. *Macromolecules* **1987**, *20*, 1384.
(92) Schick, C.; Nedbal, J. *Prog. Colloid Polym. Sci.* **1988**, *78*, 9.
(93) Schick, C.; Donth, E. *Phys. Scr.* **1991**, *43*, 423.
(94) Nouvel, O.; Seytre, G. In *Polyimides and Other High Temperature Polymers*; Abadie, M. J. M., Sillion, B., Eds.; Elsevier: Amsterdam, 1991; p 447.
(95) Mandelkern, L. *The Structure of Crystalline Polymers*, presented at the NATO Advanced Research Workshop on Polymer Crystallization, Mons, Belgium, Sept 7–11, 1992.